

SIZE AND GEOMETRY OPTIMIZATION OF TRUSS STRUCTURES USING HGPG ALGORITHM

F. Biabani, A. A. Dehghani, S. Shojaee^{*,†}, and S. Hamzehei-Javaran

Department of Civil Engineering, Shahid Bahonar University of Kerman, Kerman, Iran

ABSTRACT

Optimization has become increasingly significant and applicable in resolving numerous engineering challenges, particularly in the structural engineering field. As computer science has advanced, various population-based optimization algorithms have been developed to address these challenges. These methods are favored by most researchers because of the difficulty of calculations in classical optimization methods and achieving ideal solutions in a shorter time in metaheuristic technique methods. Recently, there has been a growing interest in optimizing truss structures. This interest stems from the widespread utilization of truss structures, which are known for their uncomplicated design and quick analysis process. In this paper, the weight of the truss, the cross-sectional area of the members as discrete variables, and the coordinates of the truss nodes as continuous variables are optimized using the HGPG algorithm, which is a combination of three metaheuristic algorithms, including the Gravity Search Algorithm (GSA), Particle Swarm Optimization (PSO), and Gray Wolf Optimization (GWO). The presented formulation aims to improve the weaknesses of these methods while preserving their strengths. In this research, 15, 18, 25, and 47-member trusses were utilized to show the efficiency of the HGPG method, so the weight of these examples was optimized while their constraints such as stress limitations, displacement constraints, and Euler buckling were considered. The proposed HGPG algorithm operates in discrete and continuous modes to optimize the size and geometric configuration of truss structures, allowing for comprehensive structural optimization. The numerical results show the suitable performance of this process.

Keywords: HGPG algorithm; Structural Optimization; Metaheuristic Algorithm; Size Optimization; Geometry Optimization; Multi-objective Optimization; Truss Design.

Received: 16 August 2024; Accepted: 22 September 2024

^{*}Corresponding author: Department of Civil Engineering, Shahid Bahonar University of Kerman, Kerman, Iran

[†]E-mail address: saeed.shojaee@uk.ac.ir (Saeed Shojaee)

1. INTRODUCTION

Finding a quick, short, and economical way to achieve the best results is the aim of optimization. It is a fundamental concept that is widely used in various fields such as engineering, economics, and computer science. However, many problems that need optimization have a large search space or complex constraints, making finding the optimal solution challenging.

Metaheuristic methods are a class of optimization algorithms that are designed to solve these types of problems. These algorithms are based on the idea of imitating natural or artificial processes, such as the behavior of ants, bees, or genetic mutations, to explore the search space efficiently and effectively. Metaheuristics have been applied to various optimization problems, including engineering design, resource allocation, and scheduling. With the rapid development of computer technology, metaheuristic methods have become more popular and have proven to be effective in solving complex optimization problems. Nowadays, optimization plays a crucial role in meeting human needs. Among the applications of optimization in engineering sciences, we can mention its use in the design of structures in civil engineering. The purpose is to reduce the weight of the structure and as a result of that reduce the economic costs [1]. Unlike traditional mathematical methods, metaheuristic algorithms have the remarkable ability to discover the best possible solution without relying on complex mathematical derivatives or needing a specific initial value. They achieve this with simpler and more intuitive formulas, making them a powerful tool for finding optimal solutions. Although the answer to these methods cannot be considered as the absolute best solution to the problem, they can be obtained with a simpler process and in a suitable and less time than mathematical methods [2]. Optimization algorithms are extensively utilized in a diverse array of civil and structural engineering fields, playing a pivotal role in enhancing efficiency and performance across various applications.

Among the research records in the field of structural optimization, there are cases such as the Modified Adolescent Identity Search Algorithm (MAISA) for optimizing the weight of steel frame structures and large-scale problems by Dehghani et al [3,4]. SeyedOskouei et al introduced the improved Artificial Rabbits Optimization algorithm (I-ARO) and utilized it for truss optimization [5]. The proposed algorithm HTC is a hybrid of two methods based on Teaching–Learning-Based Optimization (TLBO) and Charged System Search (CSS) by Dastan et al [6,7]. Optimizing the weight of truss structures using the presented method HGPG, hybridizing the three methods of Gravity Search Algorithm (GSA), Particle Swarm Optimization (PSO), and Gray Wolf Optimizer (GWO) algorithm by Biabani et al [8]. Optimizing the weight of truss structures using the CGPGC method, hybridizing GSA, PSO, GWO, and Cellular Automation method (CA) by Biabani et al [9]. Optimal design of trusses with mixed variables using Hybrid Algorithm for Sizing and Layout Optimization of Truss Structures Combining Discrete PSO and Convex Approximation (IDPSO and MMA) by Shojaei et al [10]. Shahrouzi and Taghavi developed the Modified Sine-Cosine Algorithm (MSCA) for engineering problems [11]. Optimizing the size and geometry of truss structures using the combination of DNA calculation algorithm and General Convex Approximation (GCA) method by Darvishi and Shojaei [12]. The geometry and cross-sectional area of truss members with a specific topology using the genetic algorithm by Wu and Chiu [13], Hasanchabi and Erbatur [14], and Kaveh and Kalatjari [15]. Optimizing the size of the truss

structure using the ECBO method by Kaveh et al [16]. Optimizing the weight of the structure using colliding bodies algorithms was pointed out by Kaveh and Mahdavi [17]. Today, the utilization of metaheuristic algorithms in Structural Health Monitoring (SHM) is another attractive application of these methods for solving real-world problems. For example, Mahdavi et al employed metaheuristic algorithms for Optimal Sensor Placement (OSP) and impact identification [18–20]. Mahdavi and Kaveh used metaheuristic algorithms for damage identification [21].

In recent years, size and geometry optimization of trusses has become an attractive issue. Therefore, several techniques have been presented in this theme. It is important to note that the formulation of the problem affects the optimum solution. Weak and unfit formulations cause unreliable or uneconomical designs. A suitable formulation considers geometry limitations and other constraints like displacement, stress, and Euler's buckling constraint to minimize weight and structural costs [1]. Size optimization means finding the optimal cross-section of the truss members or frames in a skeletal structure or finding the appropriate distribution of thickness in a shell structure so that the weight of the structure has the least value and the stiffness of the structure satisfies all the constraints of the problem [22]. Also, a structure can be optimized by reducing the number of nodes and elements or finding suitable coordinates of nodes. In size optimization, the design variables are cross-sections of members while in geometry optimization, the target is to find the optimal coordinate of nodal points in the design domain in such a way that its performance is maximum. In this research, the simultaneous optimization of the size and geometry of truss structures has been done by using the HGPG algorithm. The cross-sectional areas of the members are considered as discrete variables and the range of changes in the coordinates of the nodes in different directions (X, Y, Z) are considered as continuous variables.

The paper provides a brief background of fundamental concepts underlying the HGPG method in section 2. The third section offers a detailed review of the HGPG formulation and the simultaneous optimization of truss structures' size and geometry. Section 4 presents the measurement of the method's efficiency through numerical examples and a comprehensive comparative analysis with other methodologies. Finally, the paper culminates in a thorough discussion of the conclusions and their broader implications in the final section.

2. BASIC IDEAS

The HGPG algorithm is a combination of three metaheuristic methods: PSO, GSA, and GWO, which were introduced by Eberhart and James Kennedy [23], Rashedi et al [24], and Ali Mirjalili et al [25] respectively. This hybridization allows for the exploitation of the advantages of each method while minimizing their limitations. A standout feature of this method is its capacity to effectively balance exploration (global search) and exploitation (local search) during the optimization process. This is achieved through the use of a stable scheme that frequently adjusts the limit of each parameter.

Before introducing the HGPG optimization method, the article briefly outlines the core principles behind the PSO, GSA, and GWO methods. This allows the reader to better understand how the HGPG method integrates these three methods to enhance the optimization process. The PSO algorithm is a population-based optimization method that

uses the concept of swarm intelligence to search for the optimal solution. GSA, on the other hand, is a gravity-based algorithm that mimics the behavior of celestial objects to perform optimization. Lastly, GWO is inspired by the hunting behavior of grey wolves and uses a hierarchical structure to perform optimization.

The combination of PSO, GSA, and GWO in the HGPG algorithm forms a highly robust and efficient optimization framework. This approach allows for the optimization of both size and geometry simultaneously in truss structures, which is a challenging problem in engineering. Testing on standard optimization benchmarks has demonstrated that the HGPG algorithm outperforms other optimization techniques in terms of accuracy and efficiency. Its superior performance highlights the algorithm's high potential for addressing complex engineering optimization problems. The HGPG algorithm's capacity to effectively manage multiple constraints and deliver high-quality solutions positions it as a valuable tool for advanced optimization applications.

3. THE PROPOSED METHOD: HYBRID GRAVITY SEARCH, PARTICLE SWARM, AND GRAY WOLF ALGORITHM (HGPG)

The HGPG algorithm, introduced by Biabani et al in 2022 [8], incorporates the strengths and mitigates the limitations of multiple optimization techniques by combining them for enhanced performance. Recognizing that each algorithm offers distinct advantages and trade-offs, hybridization or the use of advanced computational methods has become a common approach to achieve superior outcomes. In the development of the HGPG algorithm, the GSA (Gravitational Search Algorithm) serves as the foundational framework due to its capability to leverage collective intelligence for locating optimal solutions within both vector and multidimensional spaces. GSA operates by allowing particles to move in a systematic and classical manner within a gravitational field, governed by their masses. The force exerted between particles functions as a communication signal, guiding their movements and ultimately determining their positions in the search space. This interaction enables particles to intelligently explore and exploit the search space to converge on an optimal solution. One of the key features of GSA is its consideration of both active and passive gravitational mass for each particle, which allows for the measurement and interaction of gravitational forces without reliance on problem-specific parameters. This parameter-free nature makes it adaptable across a wide range of optimization problems. The proposed HGPG algorithm builds upon this gravitational law while integrating the top three search factors of the GWO (Grey Wolf Optimizer) and the velocity calculation mechanism from PSO (Particle Swarm Optimization) to further enhance search performance.

The hybrid method has shown impressive results by optimizing both the weight and geometry of truss structures at the same time, handling continuous and discrete variables effectively. Additionally, the method demonstrates excellent convergence speed towards the global optimum. In this section, a detailed explanation of the HGPG algorithm has been presented and explores its application for the simultaneous optimization of weight and geometry in truss structures.

3.1 The HGPG Algorithm

One possible approach to determine $F_{ij}^d(t)$, which indicates the force transmitted from mass i to mass j at time t and dimension d , is to utilize,

$$F_{ij}^d(t) = G(t) \frac{M_{pi}(t) \times M_{aj}(t)}{R_{ij}(t)^{Rpower} + \varepsilon} (x_j^d(t) - x_i^d(t)) \quad (1)$$

At time t , $Rpower$ is a constant value of 0.1 and is a tiny value, while $G(t)$ represents the constant of gravity. $M_{pi}(t)$ refers to the passive gravitational mass of i and $M_{aj}(t)$ refers to the active gravitational mass of j . R_{ij} is the Euclidean distance between the two masses i and j in the equation.

$$R_{ij}(t) = \|x_i(t) - x_j(t)\|_2 \quad (2)$$

The expression for the coefficient $G(t)$ is given below:

$$G(t) = \ln\left(\frac{iter}{max - iter}\right) \quad (3)$$

In this regard, $max - iter$ represents the iterations' maximum number and $iter$ represents the iterations' current number. Employing this coefficient eliminates the necessity to modify the fixed coefficients that are integral to the $G(t)$ formula utilized in the GSA algorithm, providing an additional benefit to the algorithm being proposed. Therefore, to calculate all of the forces acting on the mass i at time t and at dimension d , and considering a random coefficient in the interval $[0,1]$, we can write,

$$F_i^d(t) = \sum_{j=1}^N rand_j F_{ij}^d(t) \quad (4)$$

In order to enhance the algorithm's ability to discover more optimal solutions, only the set of top-performing members is permitted to impact the other members.

$$F_i^d(t) = \sum_{j \in nbest, j \neq i} rand_j F_{ij}^d(t) \quad (5)$$

The value of $nbest$ is determined by using the following formula:

$$nbest = np(2 + (1 - iter / (max - iter)) * (Cp - 2)) / 100 \quad (6)$$

where cp is a fixed number and np is the particle number. After determining $nbest$, the acceleration of the objects in dimension d can be calculated using the following formula. As per Newton's second law, the acceleration of an object is equal to the net force acting on the object divided by the object's mass, and can be expressed as follows:

$$a_i^d(t) = \frac{F_i^d(t)}{M_{ii}(t)} \quad (7)$$

Here, $M_{ii}(t)$ refers to the inertial mass of the i -th particle. The equation makes use of stochastic coefficients to ensure that particle movement in the search space remains random.

$$M_{ii}(t) = M_{pi}(t) = M_{ai}(t) = M_i(t) \quad , \quad i = 1, 2, \dots, N \quad (8)$$

$$m_i(t) = \frac{value_i(t) - worst(t)}{best(t) - worst(t)} \quad (9)$$

$$M_i(t) = \frac{m_i(t)}{\sum_{j=1}^N m_j(t)} \quad (10)$$

Based on the aforementioned points, the algorithm's efficiency can be enhanced by computing the velocity in three steps, inspired by the third step of the PSO algorithm. The first step involves calculating the velocity by summing the previous velocities with the gravitational force, using the following equation:

$$v_i^d(t+1) = rand \times v_i^d(t) + a_i^d(t) \quad (11)$$

Next, in the second step, the velocity calculated in the first step is updated using the following equation:

$$v_i^d(t+1) = rand \times v_i^d(t) + C_k \times a(t) + (2 - C_k) \times x_{mean-gbest}^d - x_i^d(t) \quad (12)$$

The value of the coefficient C_k is obtained by using the following equation:

$$C_k = 2 - 0.25 \times \log \frac{ncn}{t} \quad (13)$$

Furthermore, the initial value of ncn is set to 1 and added to the initial population at all times. Finally, the PSO method is used with the velocity calculated in the previous step.

$$V_i^d(t+1)_{IGSA} = \beta V_i^d(t)_{GSA} + C_1 \times \varphi_1 \times (x_{pbest_i}^d - x_i^d(t)) + C_2 \times \varphi_2 \times (x_{gbest}^d - x_i^d(t)) \quad (14)$$

where, β , φ_1 and φ_2 are random variables in the range [0,1] and C_1 and C_2 are constant coefficients. In addition, since the GWO algorithm considers the effect of the top 3 particles to find the best solution, $x_{mean-gbe}^d$ is used instead of x_{gbest}^d in the PSO formula, to use this point in the proposed algorithm in the velocity part.

$$X_{mean-gbest}^d = (X_{alpha}^d + X_{beta}^d + X_{delta}^d) / 3 \quad (15)$$

where, x_{alpha}^d , x_{beta}^d , and x_{delta}^d represent the top 3 particles position in the algorithm. Therefore, the new position of each particle can be calculated as the sum of the calculated values using vector summation.

$$x_i^d(t+1) = x_i^d(t) + v_i^d(t+1) \quad (16)$$

The algorithm has been upgraded to get rid of the underperforming particle and replace it with a better one. To make this happen, a random value is generated after identifying the weakest particle, known as the *gamma* particle. If the randomly generated value is lower than a computed value based on the current iteration and the maximum number of iterations, the *gamma* particle's value is replaced with a new one. Otherwise, it is substituted with the average value of the x_{α}^d , x_{β}^d , and x_{δ}^d particles. The HGPG method is summarized in pseudocode 1.

Pseudocode 1: The HGPG algorithm

-
- 1: **Initialize** particles with random solutions
 - 2: **Evaluate** the fitness of each particle
 - 3: **Set** the initial best positions of each particle and the global best position found by any particle
 - 4: **Repeat** until the stopping criteria are satisfied:
 - 5: **Calculate and update** the particle's mass and particle's force.
 - 6: **Determine** the superior alpha, beta, and delta particles
 - 7: **Calculate and update** the velocity of particles.
 - 8: **Update** the position of particles.
 - 9: **Evaluate** the fitness of each particle
 - 10: **Update** the best positions if the current solution is better
 - 11: **Update** the global best position if a better solution is found
 - 12: **Return** the best solution found
-

3.2 Simultaneously Optimization of Discrete and Continuous Variables

In the optimization of truss structures for size, the objective is to minimize the weight of the structure by taking into account the cross-sectional area of the truss members as design variables, while ensuring that the problem's constraints are met. In some cases, various aspects of the cross-section are considered as design variables. For instance, when addressing column buckling, the design variables include the cross-sectional area and moment of inertia of the cross-section. It is crucial to note that these cross-sectional areas are typically treated as discrete variables, reflecting the fact that, in practical design scenarios, truss structures are constructed using standard steel profiles available in the market. These profiles come in a predefined, discrete set of cross-sectional areas, from which the most suitable ones must be selected. Consequently, the size optimization process focuses on selecting the best possible combination of these predefined profiles to achieve the desired structural performance with minimal weight.

Geometric optimization of truss structures involves minimizing the weight of truss structures while working within given constraints, using the coordinates of the truss nodes as design variables. In this form of optimization, the node coordinates are treated as continuous variables since they can take any value from a range of real numbers, allowing for flexibility in adjusting the positioning of nodes and consequently altering the lengths of truss elements. Through this process, an efficient and lightweight truss structure with an ideal configuration can be achieved. In optimization, the geometry of the design set is not fixed and is usually considered as a continuous variable, and only the boundaries of the design domain can be changed. In this study, both the cross-sectional areas of the truss members (as discrete

variables) and the node coordinates (as continuous variables) are considered for weight optimization.

To simultaneously optimize the weight and size of truss structures, the following steps are taken:

Step 1: Define the list of available profiles for cross-sections and set the index number of the profile list for the lower and upper bound of cross-sections variables. Continuous variables are applied according to the normal procedure.

Step 2: Separate cross-sectional variables from geometry variables.

Step 3: Round discrete variables to the nearest integer number and replace it with previous values.

Step 4: Choose an appropriate cross-section from the profile list according to its index number.

Step 5: Evaluate the fitness using discrete variables and continuous geometry variables.

Note that all the above steps were applied in the objective function, except step 1.

4. NUMERICAL EXAMPLES

In this section, four benchmark examples of 15, 18, 25, and 47-bar trusses have been discussed and the results of weight and geometry optimization using the HGPG method have been compared with those obtained from other similar methods. In the following examples, the standard deviations (Std) are calculated from 30 independent runs. The control parameters are considered in Table 1.

Table 1: Controlling parameters

| Parameter | Description | Value |
|---------------------------------|------------------------|-------|
| R power | Power of R coefficient | 0.01 |
| W | Initial weight | 0.9 |
| C ₁ , C ₂ | Learning coefficient | 2 |
| Number of Run | – | 30 |

4.1. Fifteen-bar Truss

The study's first example involves analyzing a 15-bar truss that's under a concentrated load of $P = -10$ ksi applied at node 8 (see Figure 1). The material density is $\rho = 0.1$ lb/in³, and the modulus of elasticity is $E = 10000$ ksi. Cross-sections are chosen from a range of available profiles in Table 2, with allowable tensional and compressive stress limited to 25 ksi. For more design details, refer to Table 2. The HGPG method is compared with similar algorithms in Table 3. Stress values for each truss element are presented in Table 4, and Figure 2 illustrates that stress ratios for all elements are within the allowable limit. The initial and optimized truss geometries are shown in Figure 3, while the convergence curve in Figure 4 depicts the HGPG method's convergence rate. Furthermore, Figure 5 provides insights from 30 independent runs, showcasing average weight, worst weight, and standard deviation at 82.4, 87.76, and 2.8 lb, respectively.

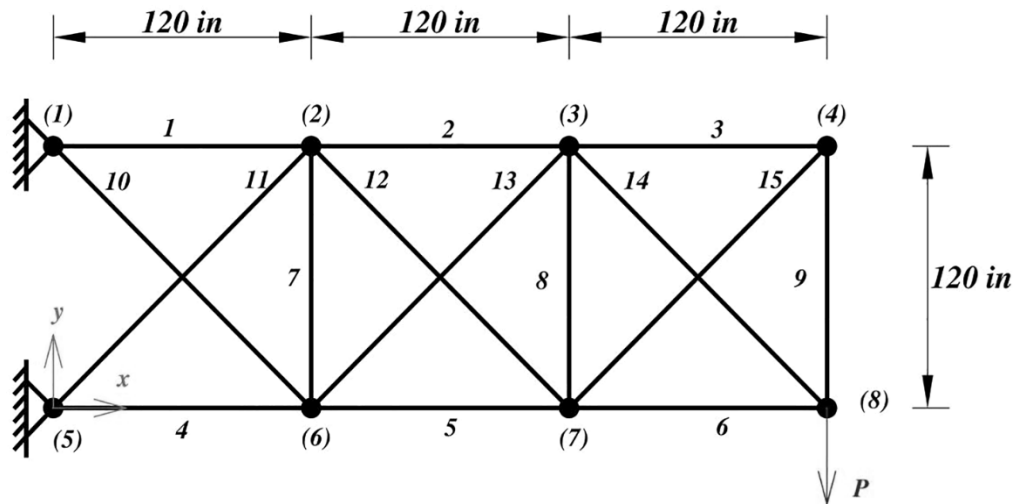


Figure 1: Initial Geometry and node numbers of the 15-bar truss

Table 2: The primary data of the 15-bar truss

| Loading data | Node | F_x (Kips) | F_y (Kips) | F_z (Kips) |
|--------------------------------|--|--------------|--------------|--------------|
| | 8 | 0 | -10 | 0 |
| Design variables | Size variables $A_1; A_2; A_3; A_4; A_5; A_6;$ $A_7; A_8; A_9; A_{10}; A_{11};$ $A_{12}; A_{13}; A_{14}; A_{15}$ | | | |
| | Geometry variables $x_2 = x_6; x_3 = x_7; y_2; y_3; y_4; y_6; y_7; y_8$ | | | |
| Constraint data | Stress constraints $(\sigma_i)_i \leq 25 \text{ Ksi}; \quad i=1,2,\dots,15$ $ (\sigma_c)_i \leq 25 \text{ Ksi}; \quad i=1,2,\dots,15$ | | | |
| | Side constraints of geometry variables $100 \text{ in} \leq x_2 \leq 140 \text{ in}$ $220 \text{ in} \leq x_3 \leq 260 \text{ in}$ $100 \text{ in} \leq y_2 \leq 140 \text{ in}$ $100 \text{ in} \leq y_3 \leq 140 \text{ in}$ $50 \text{ in} \leq y_4 \leq 90 \text{ in}$ $-20 \text{ in} \leq y_6 \leq 20 \text{ in}$ $-20 \text{ in} \leq y_7 \leq 20 \text{ in}$ $20 \text{ in} \leq y_8 \leq 60 \text{ in}$ | | | |
| List of the available profiles | $A_i \in S = \{0.111, 0.141, 0.174, 0.22, 0.27, 0.287, 0.347, 0.44, 0.539, 0.954, 1.081, 1.174, 1.333, 1.488, 1.764, 2.142, 2.697, 2.8, 3.131, 3.565, 3.813, 4.805, 5.952, 6.572, 7.192, 8.525, 9.3, 10.85, 13.33, 14.29, 17.17, 19.18\} \text{ in}^2$ | | | |

Table 2: Comparison of optimized designs for the 15-bar truss

| | Design variables | ARSAGA [26] | Improved GA [27] | CPSO [28] | DNA-GCA [12] | Present work |
|----------------------------------|------------------|-------------|------------------|-----------|--------------|--------------|
| Size variables (in^2) | A_1 | 0.954 | 1.081 | 1.174 | 1.081 | 0.954 |
| | A_2 | 1.081 | 0.539 | 0.539 | 0.539 | 0.539 |
| | A_3 | 0.44 | 0.287 | 0.347 | 0.27 | 0.287 |
| | A_4 | 1.174 | 0.954 | 0.954 | 0.954 | 1.333 |
| | A_5 | 1.488 | 0.954 | 0.954 | 0.954 | 0.539 |
| | A_6 | 0.27 | 0.22 | 0.141 | 0.22 | 0.174 |
| | A_7 | 0.27 | 0.111 | 0.141 | 0.111 | 0.22 |
| | A_8 | 0.347 | 0.111 | 0.111 | 0.111 | 0.111 |
| | A_9 | 0.22 | 0.287 | 1.174 | 0.27 | 0.27 |

| | | | | | | |
|-------------------------|------------------------|---------|---------|---------|---------|---------|
| | A ₁₀ | 0.44 | 0.22 | 0.141 | 0.287 | 0.539 |
| | A ₁₁ | 0.22 | 0.44 | 0.44 | 0.44 | 0.22 |
| | A ₁₂ | 0.44 | 0.44 | 0.44 | 0.287 | 0.111 |
| | A ₁₃ | 0.347 | 0.111 | 0.141 | 0.141 | 0.44 |
| | A ₁₄ | 0.27 | 0.22 | 0.141 | 0.27 | 0.22 |
| | A ₁₅ | 0.22 | 0.347 | 0.347 | 0.27 | 0.287 |
| Geometry variables (in) | x ₂ | 118.346 | 133.612 | 102.287 | 123.529 | 103.423 |
| | x ₃ | 225.209 | 234.752 | 240.505 | 239.110 | 259.743 |
| | y ₂ | 119.046 | 100.449 | 112.584 | 123.791 | 131.452 |
| | y ₃ | 105.086 | 104.738 | 108.043 | 115.211 | 117.221 |
| | y ₄ | 63.375 | 73.762 | 57.795 | 72.968 | 53.347 |
| | y ₆ | -20 | -10.067 | -6.430 | -8.153 | 8.568 |
| | y ₇ | -20 | -1.339 | -1.801 | 3.896 | 16.659 |
| | y ₈ | 57.722 | 50.402 | 57.799 | 42.603 | 53.328 |
| Results | W _{best} (lb) | 104.573 | 79.82 | 77.615 | 79.807 | 77.604 |
| | Analysis | N/A | 8000 | 4500 | N/A | 6980 |

Table 3: The stress value of the 15-bar truss

| Member | Stress (lb/in ²) | Member | Stress (lb/in ²) |
|--------|------------------------------|--------|------------------------------|
| 1 | 22020.10 | 9 | 21915.66 |
| 2 | 24998.75 | 10 | 24873.83 |
| 3 | 24372.13 | 11 | 24998.75 |
| 4 | -22582.72 | 12 | 22171.57 |
| 5 | -22206.45 | 13 | -24706.26 |
| 6 | -24908.52 | 14 | 21939.49 |
| 7 | -24949.17 | 15 | -21887.95 |
| 8 | 14163.02 | | |

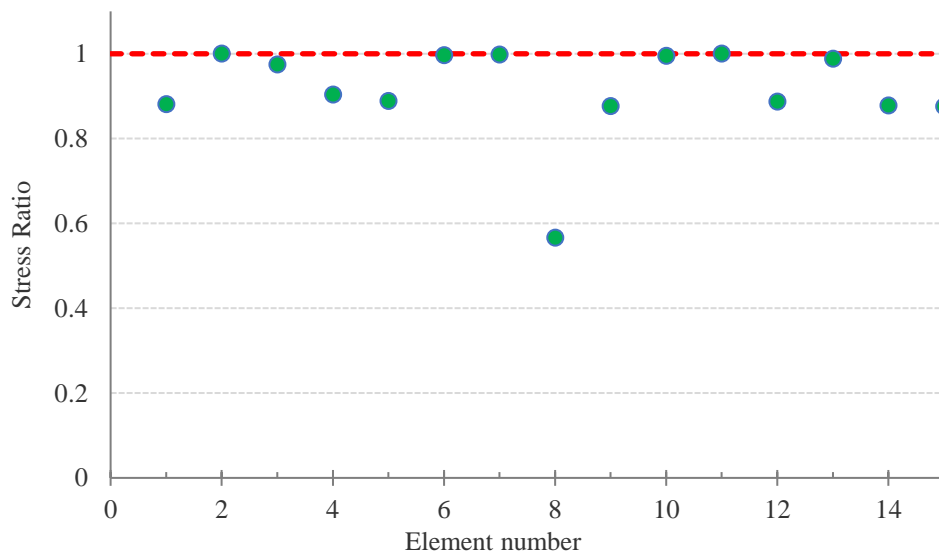


Figure 2: The stress ratio of the 15-bar truss in the optimal solution

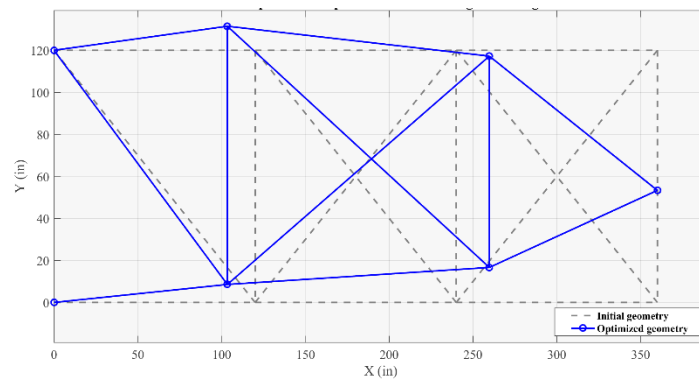


Figure 3: Initial and optimum geometry of the 15-bar truss

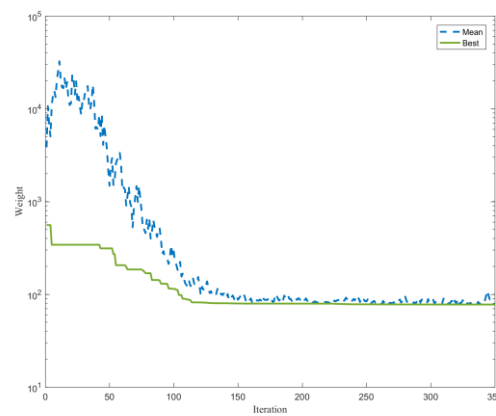


Figure 4: The convergence curve of the 15-bar truss

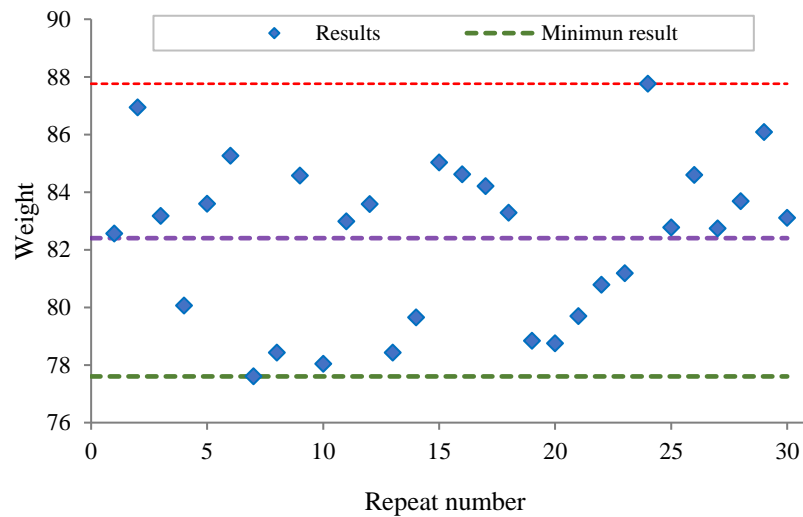


Figure 5: The optimal weight of the 15-bar truss in each independent run

4.2. Eighteen-bar Truss

The 18-bar truss with 12 variables has been illustrated in Figure 6. The material density is $\rho = 0.1 \text{ lb/in}^3$ and the module of elasticity is $E = 10000 \text{ ksi}$. The truss elements are categorized into 4 groups and their cross-sections are selected from the set of $A_i \in S = \{2.00, 2.25, \dots, 21.50, 21.75\} \text{ in}^2$. A concentrated load $P = -20 \text{ ksi}$ was applied at nodes 1, 2, 4, 6, and 8. The allowable tensional and compressive stress is limited to 20 Ksi, and the Euler buckling stress constraints should be considered. Other design information is summarized in Table 5. Upon reviewing Table 6 data, the HGPB method optimized the 18-bar truss by approximately 5.6 lb, outperforming the ABC algorithm. The stress value of each element is presented in Table 7, and Figure 7 depicts the stress ratios. The initial and optimized geometry of the 18-bar is illustrated in Figure 8, while the convergence curve of the best run is presented in Figure 9. Additionally, Figure 10 displays the optimal outcome of the 18-bar in each independent run. The average weight, the worst weight, and the standard deviation were calculated to be 4651.65 lbs, 5058.32 lbs, and 107.62 lbs, respectively.

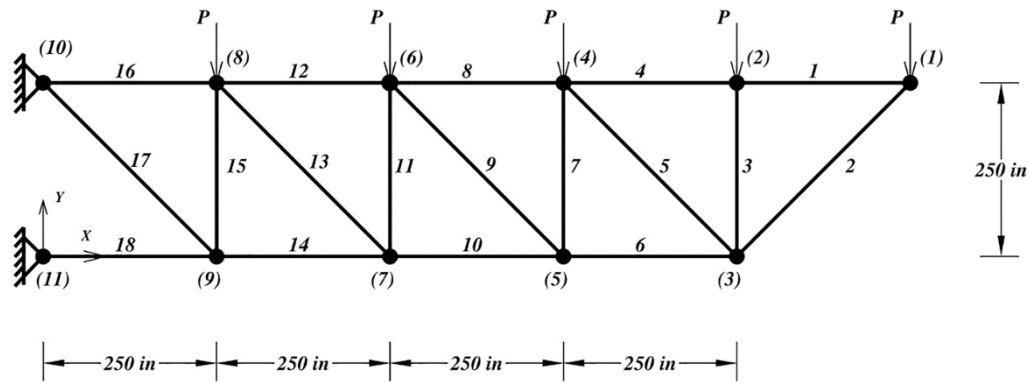


Figure 6: Initial Geometry and node numbers of the 18-bar truss

Table 5: The primary data of the 18-bar truss

| | Node | F_x (kips) | F_y (kips) | F_z (kips) |
|------------------|---|--------------|---------------------------------|--------------|
| Loading data | 1 | 0 | -20 | 0 |
| | 2 | 0 | -20 | 0 |
| | 4 | 0 | -20 | 0 |
| | 6 | 0 | -20 | 0 |
| | 8 | 0 | -20 | 0 |
| Design variables | Size variables | | Geometry variables | |
| | $A_1= A_4= A_8= A_{12}= A_{16}; A_2=$ | | $x_3; y_3; x_5; y_5; x_7; y_7;$ | |
| | $A_6= A_{10}= A_{14}= A_{18}; A_3= A_7=$ | | $x_9; y_9$ | |
| | $A_{11}= A_{15};$ $A_5= A_9= A_{13}= A_{17}$ | | | |
| Constraint data | Stress constraints | | | |
| | $(\sigma_i)_i \leq 20 \text{ Ksi};$ | | $i=1,2,...,18$ | |
| | $ (\sigma_c)_i \leq 20 \text{ Ksi};$ | | $i=1,2,...,18$ | |
| | Euler buckling stress constraints | | | |
| | $ (\sigma_c)_i \leq \alpha A_i E/L_i^2, \alpha=4;$ | | $i=1,2,...,18$ | |
| | Side constraints of geometry variables | | | |
| | $775 \text{ in} \leq x_3 \leq 1225 \text{ in}$ | | | |
| | $-225 \text{ in} \leq y_3 \leq 245 \text{ in}$ | | | |
| | $525 \text{ in} \leq x_5 \leq 975 \text{ in}$ | | | |

-225 in $\leq y_5 \leq$ 245 in
 275 in $\leq x_7 \leq$ 725 in
 -225 in $\leq y_7 \leq$ 245 in
 25 in $\leq x_9 \leq$ 475 in
 -225 in $\leq y_9 \leq$ 245 in

List of the available profiles $A_i \in S = \{2.00, 2.25, \dots, 21.50, 21.75\} \text{ in}^2$

Table 4: Comparison of optimized designs for the 18-bar truss

| | Design variables | Rajeev and Krishnamoorthy [29] | Yang [30] | CPSO [28] | D-ICDE [31] | ABC [32] | Present work |
|-----------------------------------|------------------------|--------------------------------|-----------|-----------|-------------|----------|--------------|
| Size variables (in ²) | A ₁ | 12.5 | 12.61 | 12 | 13 | 12.5 | 12 |
| | A ₂ | 16.25 | 18.1 | 17.25 | 17.5 | 17.75 | 17.75 |
| | A ₃ | 8 | 5.47 | 6.25 | 6.5 | 5.75 | 5.5 |
| | A ₄ | 4 | 3.54 | 4.75 | 3 | 3.75 | 4.5 |
| Geometry variables (in) | x ₃ | 891.9 | 914.5 | 902.914 | 914.06 | 912.997 | 909.864 |
| | y ₃ | 145.3 | 183 | 174.72 | 183.46 | 183.681 | 414.602 |
| | x ₅ | 610.6 | 647 | 632.713 | 640.53 | 642.714 | 642.853 |
| | y ₅ | 118.2 | 147.4 | 141.296 | 133.74 | 143.892 | 203.123 |
| | x ₇ | 385.4 | 414.2 | 407.132 | 406.12 | 411.692 | 183.984 |
| | y ₇ | 72.5 | 100.4 | 85.933 | 92.63 | 97.148 | 148.806 |
| | x ₉ | 184.4 | 200 | 197.672 | 196.69 | 200.909 | 96.533 |
| | y ₉ | 23.4 | 31.9 | 19.809 | 37.06 | 30.219 | 22.228 |
| Results | W _{best} (lb) | 4616.8 | 4552.8 | 4561.131 | 4554.29 | 4537.064 | 4531.467 |
| | Analysis | N/A | N/A | 4500 | 8025 | 2700 | 9975 |

Table 5: The stress value of the 18-bar truss

| Member | Stress (lb/in ²) | Member | Stress (lb/in ²) |
|--------|------------------------------|--------|------------------------------|
| 1 | 8587.17 | 10 | -12948.26 |
| 2 | -5913.75 | 11 | -5970.43 |
| 3 | -6154.17 | 12 | 19999.91 |
| 4 | 10862.77 | 13 | -1023.80 |
| 5 | 10075.22 | 14 | -14130.17 |
| 6 | -9788.61 | 15 | -3129.38 |
| 7 | -9878.43 | 16 | 20008.23 |
| 8 | 17646.57 | 17 | 20000.00 |
| 9 | 3342.32 | 18 | -17002.31 |

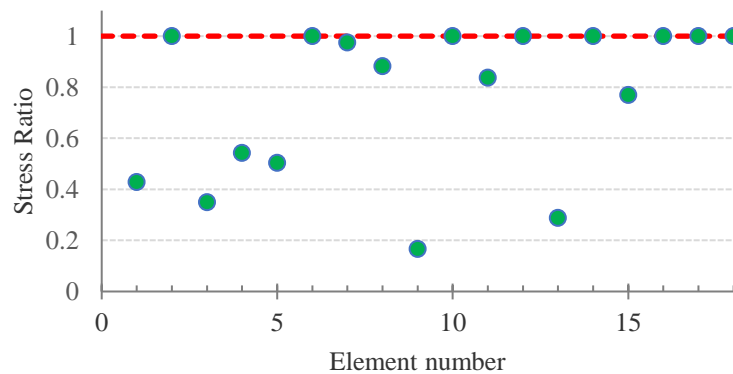


Figure 7: The stress ratio of the 18-bar truss in the optimal solution

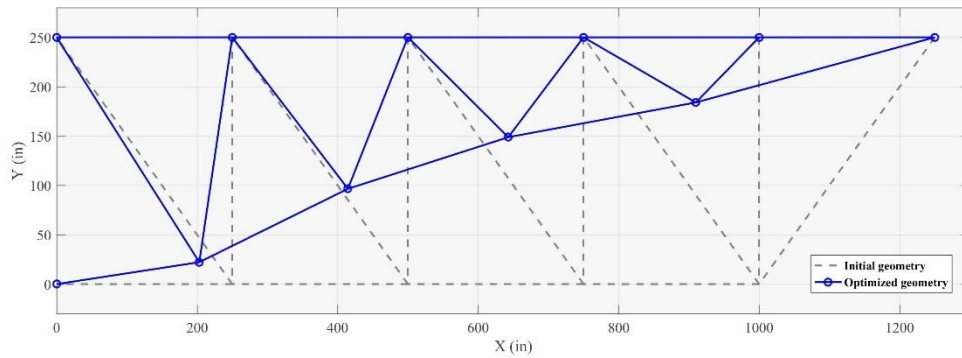


Figure 8: Initial and optimum geometry of the 18-bar truss

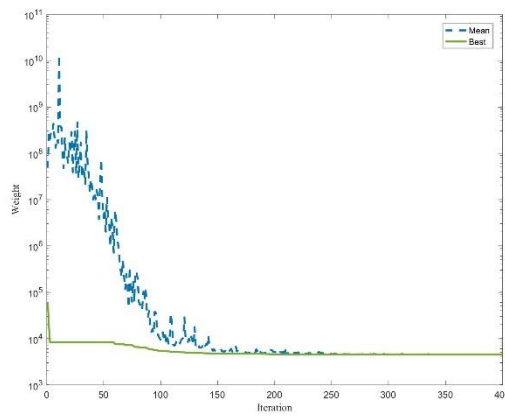


Figure 9: The convergence curve of the 18-bar truss

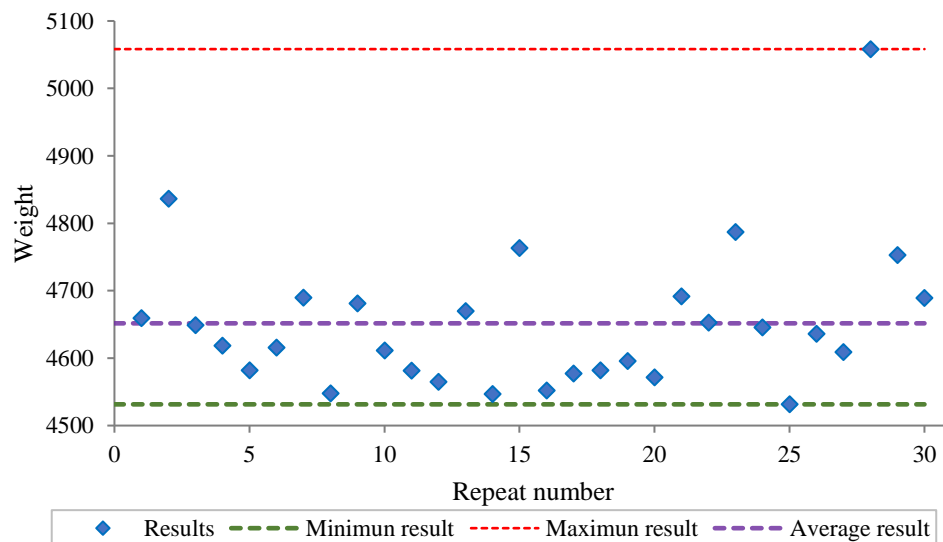


Figure 10: The optimal weight of the 18-bar truss in each independent run

4.3. Twenty-five-bar Truss

The 25-bar truss with 8 cross-sectional variables and 5 geometrical variables is considered for the third example. The geometry and the node numbers are shown in Figure 11, and the nodal coordinates are defined in Table 8. The 25-bar truss has a 0.89 cm displacement constraint of all nodes in all directions. The grouped members are in Table 9. The allowable stress is 275.8 Mpa for tension and compression stresses. The material density and the module of elasticity are 2720 kg/m³ and 68.95 Gpa, respectively. Other necessary data for design are summarized in Table 10. Table 11 exhibits the comparison of the HPGP method results with similar approaches. The stress of each member and displacement of each node obtained from the best design are shown in Table 12 and Table 13, respectively. The stress ratios are shown in Figure 12. The stress ratio has decreased due to displacement constraints. The initial and optimized geometry of the 25-bar truss and the convergence curve of the best run has been shown in Figure 13 and Figure 14, respectively. the average weight came in at 55.76 lb, the worst weight was 57.41 lb, and the standard deviation was 0.806 lb. Figure 15 demonstrates the optimal weight of the 25-bar truss in each independent run.

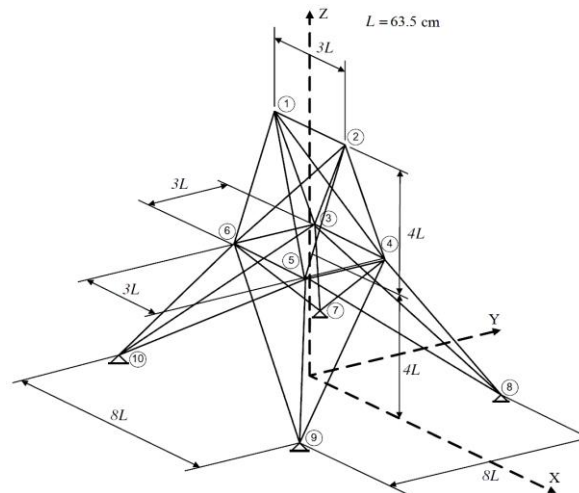


Figure 11: Initial Geometry and node numbers of the 25-bar truss

Table 6: The nodal coordinates of the 25-bar truss

| Node | x(cm) | y(cm) | z(cm) |
|------|--------|--------|-------|
| 1 | -95.25 | 0 | 508 |
| 2 | 95.25 | 0 | 508 |
| 3 | -95.25 | 95.25 | 254 |
| 4 | 95.25 | 95.25 | 254 |
| 5 | 95.25 | -95.25 | 254 |
| 6 | -95.25 | -95.25 | 254 |
| 7 | -254 | 254 | 0 |
| 8 | 254 | 254 | 0 |
| 9 | 254 | -254 | 0 |
| 10 | -254 | -254 | 0 |

Table 7: The grouping of truss elements for the 25-bar truss

| Group | Members (nodes) |
|----------------|----------------------------------|
| A ₁ | 1(1,2) |
| A ₂ | 2(1,4),3(2,3),4(1,5),5(2,6) |
| A ₃ | 6(2,5),7(2,4),8(1,3),9(1,6) |
| A ₄ | 10(3,6),11(4,5) |
| A ₅ | 12(3,4),13(5,6) |
| A ₆ | 14(3,10),15(6,7),16(4,9),17(5,8) |
| A ₇ | 18(3,8),19(4,7),20(6,9),21(5,10) |
| A ₈ | 22(3,7),23(4,8),24(5,9),25(6,10) |

Table 10: The primary data of the 25-bar truss

| | Node | F_x (kN) | F_y (kN) | F_z (kN) |
|------------------------------------|---|------------|--|--------------|
| Loading data | 1 | 4.454 | -44.537 | -44.537 |
| | 2 | 0 | -44.537 | -44.537 |
| | 3 | 2.227 | 0 | 0 |
| | 6 | 2.672 | 0 | 0 |
| Design variables | Size variables | | Geometry variables | |
| | A ₁ ; A ₂ ; A ₃ ; A ₄ ; A ₅ ; | | x ₄ = x ₅ =- x ₃ =- x ₆ ; | |
| | A ₆ ; A ₇ ; A ₈ | | y ₄ = y ₃ =- y ₅ =- y ₆ ; | |
| | | | z ₄ = z ₃ = z ₅ = z ₆ ; | |
| Constraint data | Stress constraints | | x ₈ = x ₉ =- x ₇ =- x ₁₀ ; | |
| | (σ _i) _i ≤ 275.8 Mpa; | | y ₈ = y ₇ =- y ₉ =- y ₁₀ | |
| | (σ _c) _i ≤ 275.8 Mpa; | | | |
| | Displacement constraints | | | |
| | Δ _i ≤ 0.89 cm; | | i=1,2,...,6 | |
| | | | | |
| | Side constraints of geometry variables | | | |
| | 50.8cm ≤ x ₄ ≤ 152.4cm | | | |
| | 101.6cm ≤ y ₄ ≤ 203.2cm | | | |
| | 228.6cm ≤ z ₄ ≤ 330.2cm | | | |
| 101.6cm ≤ x ₈ ≤ 203.2cm | | | | |
| 254cm ≤ y ₈ ≤ 355.6cm | | | | |
| List of the available profiles | A _i ∈ S={0.645I (I=1,2,...,26), 18.064, 19.355, 20.645, 21.935}cm ² | | | i=1,2,...,25 |

Table 8: Comparison of optimized designs for the 25-bar truss

| | Design variables | Wu and Chow [33] | Kaveh and Kalatjari [15] | Rahami et al [34] | CPSO [28] | D-ICDE [31] | Present work |
|-----------------------------------|------------------|------------------|--------------------------|-------------------|-----------|-------------|--------------|
| Size variables (cm ²) | A ₁ | 0.645 | 0.645 | 0.645 | 1.935 | 0.645 | 0.645 |
| | A ₂ | 1.29 | 0.645 | 0.645 | 0.645 | 0.645 | 0.645 |
| | A ₃ | 7.097 | 7.097 | 7.097 | 6.45 | 5.805 | 6.45 |
| | A ₄ | 1.29 | 0.645 | 0.645 | 0.645 | 0.645 | 0.645 |
| | A ₅ | 1.935 | 0.645 | 0.645 | 0.645 | 0.645 | 0.645 |
| | A ₆ | 0.645 | 0.645 | 0.645 | 0.645 | 0.645 | 0.645 |
| | A ₇ | 1.29 | 0.645 | 1.29 | 1.29 | 0.645 | 0.645 |
| | A ₈ | 5.806 | 6.452 | 5.16 | 5.805 | 6.45 | 6.45 |
| Geometry variables (cm) | x ₄ | 104.318 | 92.024 | 83.944 | 85.084 | 93.548 | 94.661 |
| | y ₄ | 135.814 | 148.742 | 136.058 | 158.429 | 148.666 | 132.172 |
| | z ₄ | 316.484 | 293.599 | 329.969 | 290.817 | 311.582 | 327.746 |
| | x ₈ | 129.032 | 118.008 | 111.208 | 101.735 | 124.993 | 126.844 |

| | | | | | | | |
|---------|------------------------|---------|---------|---------|---------|---------|---------|
| | y_8 | 333.959 | 324.993 | 347.569 | 339.522 | 347.320 | 333.469 |
| Results | W_{best} (kg) | 61.83 | 56.29 | 54.53 | 56.047 | 53.869 | 53.873 |
| | Analysis | N/A | N/A | 10000 | 4500 | 6000 | 8790 |

Table 9: The stress value of the 25-bar truss

| Member | Stress (kg/cm ²) | Member | Stress (kg/cm ²) | Member | Stress (kg/cm ²) |
|--------|------------------------------|--------|------------------------------|--------|------------------------------|
| 1 | 265.97 | 10 | 4000.63 | 19 | 6756.20 |
| 2 | -2219.10 | 11 | 5306.34 | 20 | -13216.68 |
| 3 | 3456.02 | 12 | -1499.89 | 21 | -1356.82 |
| 4 | -8541.76 | 13 | -2269.69 | 22 | 2622.83 |
| 5 | -3518.82 | 14 | -5055.08 | 23 | 850.42 |
| 6 | -9851.61 | 15 | 4574.14 | 24 | -10132.80 |
| 7 | 1294.04 | 16 | -5461.40 | 25 | -8407.42 |
| 8 | 1726.53 | 17 | 4086.20 | | |
| 9 | -9468.83 | 18 | -4495.39 | | |

Table 10: The nodal displacements of the 25-bar truss

| Node | Δx (cm) | Δy (cm) | Δz (cm) |
|------|-----------------|-----------------|-----------------|
| 1 | 0.883 | -0.890 | -0.429 |
| 2 | 0.890 | -0.881 | -0.422 |
| 3 | 0.730 | -0.443 | -0.171 |
| 4 | 0.688 | -0.414 | -0.131 |
| 5 | 0.710 | -0.617 | -0.219 |
| 6 | 0.772 | -0.596 | -0.264 |
| 7 | 0 | 0 | 0 |
| 8 | 0 | 0 | 0 |
| 9 | 0 | 0 | 0 |
| 10 | 0 | 0 | 0 |

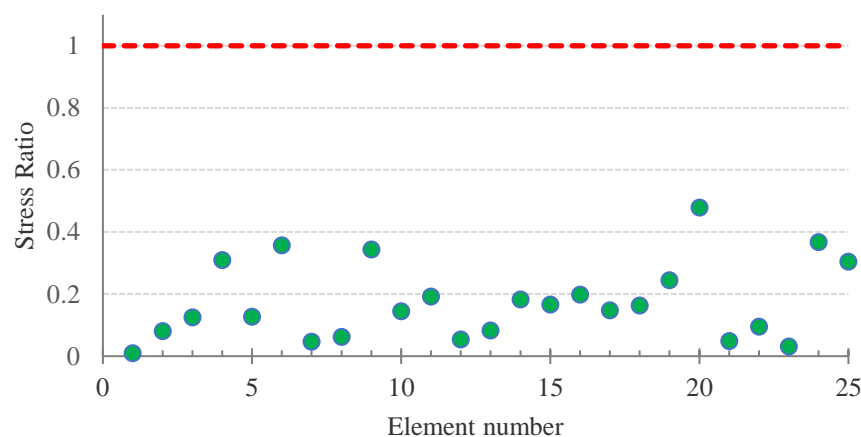


Figure 12: The stress ratio of the 25-bar truss in the optimal solution

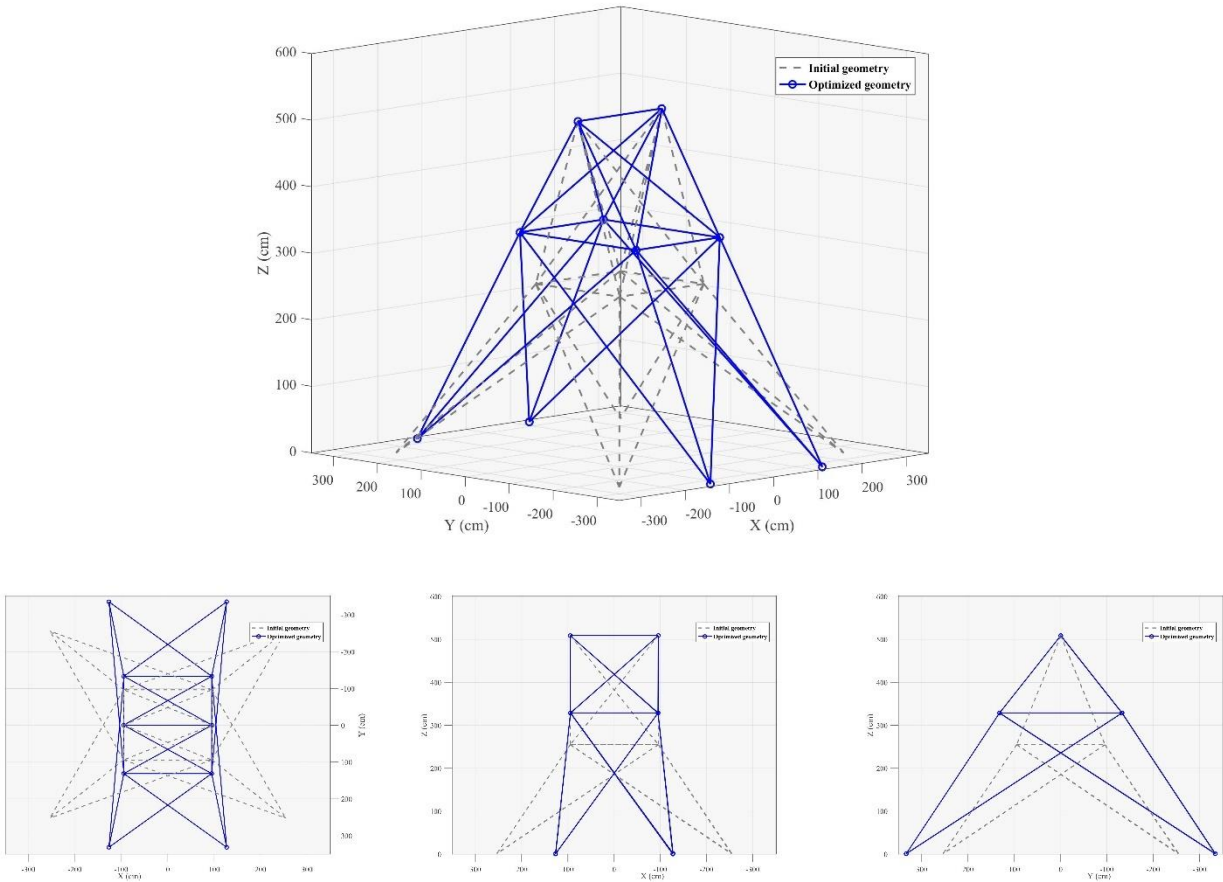


Figure 13: Initial and optimum geometry of the 25-bar truss

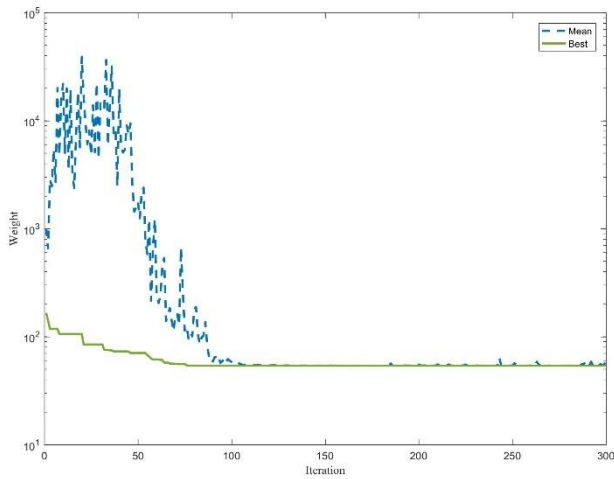


Figure 14: The convergence curve of the 25-bar truss

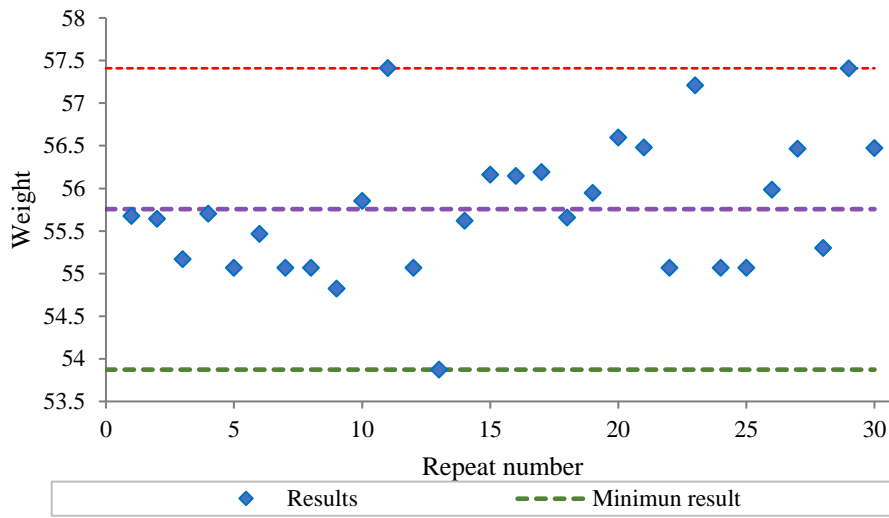


Figure 15: The optimal weight of the 25-bar truss in each independent run

4.4. Forty-seven-bar Truss

The last numerical example is the 47-bar truss (Figure 16) with 44 size and geometry variables. Truss elements are categorized into 27 groups. Table 14 exhibits the available profiles and 17 other geometric variables. The tensional stress is limited to 20 ksi and the compressive stress is limited to $\min \{15, \alpha A_i E/L_i^2\}$ ksi in which $\alpha=3.96$. The material density is $\rho=0.3$ lb/in³ and the module of elasticity is $E=30000$ ksi. All primary information is summarized in Table 14. The proposed method is compared with other similar methods in Table 15. The HGPG algorithm optimized the 47-bar truss about 7.72 lb, compared to the DNA-GCA algorithm. Similar to the previous examples, for a better understanding of the obtained stresses for each element (Table 16), the stress ratios are shown in Figure 17. The initial and optimized geometry of the 47-bar truss and the convergence curve of the best run has been shown in Figure 18 and Figure 19, respectively. According to 30 independent runs, the average weight, the worst weight, and the standard deviation were 2154.97, 2766.53, and 239.17 lb, respectively. Figure 20 shows the optimal result of the 47-bar truss in each independent run.

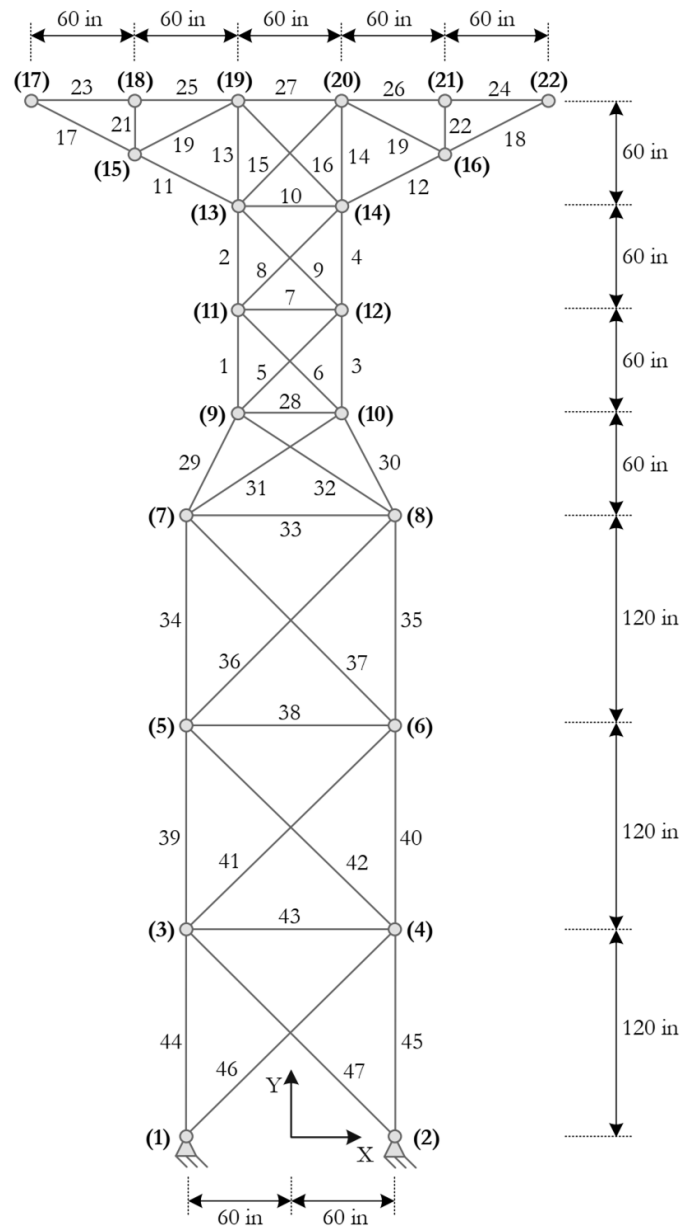


Figure 16: Initial Geometry and node numbers of the 47-bar truss

Table 14: The primary data of the 47-bar truss

| | Node | F_x (kips) | F_y (kips) | F_z (kips) |
|------------------|---|--------------|--------------|--------------|
| Loading data | 17 | 6 | -14 | 0 |
| | 22 | 6 | -14 | 0 |
| Design variables | Size variables | | | |
| | $A_3 = A_1$; $A_4 = A_2$; $A_5 = A_6$; A_7 ; $A_8 = A_9$; A_{10} ; $A_{12} = A_{11}$; | | | |
| | $A_{14} = A_{13}$; $A_{15} = A_{16}$; $A_{18} = A_{17}$; $A_{20} = A_{19}$; $A_{22} = A_{21}$; $A_{24} = A_{23}$; | | | |
| | $A_{26} = A_{25}$; A_{27} ; A_{28} ; $A_{30} = A_{29}$; $A_{31} = A_{32}$; A_{33} ; $A_{35} = A_{34}$; $A_{36} = A_{37}$; A_{38} ; $A_{40} = A_{39}$; $A_{41} = A_{42}$; | | | |

A_{43} ; $A_{45} = A_{44}$; $A_{46} = A_{47}$

| | |
|-----------------|---|
| Constraint data | Geometry variables $x_2=-x_1; x_4=-x_3; y_4=y_3; x_6=-x_5; y_6=y_5; x_8=-x_7; y_8=y_7;$ $x_{10}=-x_9; y_{10}=y_9; x_{12}=-x_{11}; y_{12}=y_{11}; x_{14}=-x_{13}; y_{14}=y_{13};$ $x_{20}=-x_{19}; y_{20}=y_{19}; x_{21}=-x_{18}; y_{21}=y_{18}$ |
| | Stress constraints $(\sigma_i)_i \leq 20 \text{ ksi}; \quad i=1,2,\dots,47$ $ (\sigma_c)_i \leq 15 \text{ ksi}; \quad i=1,2,\dots,47$ |
| | Euler buckling stress constraints $ (\sigma_c)_i \leq \alpha A_i E/L_i^2, \alpha=3.96; \quad i=1,2,\dots,47$ |
| | Side constraints of geometry variables $0 \leq x_2 \leq 150 \text{ in}$ $0 \leq x_4 \leq 150 \text{ in}$ $0 \leq y_4 \leq 240 \text{ in}$ $0 \leq x_6 \leq 150 \text{ in}$ $120 \text{ in} \leq y_6 \leq 360 \text{ in}$ $0 \leq x_8 \leq 150 \text{ in}$ $240 \text{ in} \leq y_8 \leq 420 \text{ in}$ $0 \leq x_{10} \leq 75 \text{ in}$ $360 \text{ in} \leq y_{10} \leq 480 \text{ in}$ $0 \leq x_{12} \leq 75 \text{ in}$ $420 \text{ in} \leq y_{12} \leq 540 \text{ in}$ $0 \leq x_{14} \leq 75 \text{ in}$ $480 \text{ in} \leq y_{14} \leq 600 \text{ in}$ $0 \leq x_{20} \leq 75 \text{ in}$ $540 \text{ in} \leq y_{20} \leq 660 \text{ in}$ $0 \leq x_{21} \leq 150 \text{ in}$ $540 \text{ in} \leq y_{21} \leq 660 \text{ in}$ |
| | List of the available profiles $A_i \in S=\{0.1, 0.2, 0.3, \dots, 5.0\} \text{ in}^2$ |

Table 11: Comparison of optimized designs for the 47-bar truss

| | Design variables | Hasancebi and Erbatur [35] | Salajegheh and Vanderplaats [36] | SCPSO [28] | DNA-GCA [12] | ABC [32] | Present work |
|-----------------------------------|------------------|----------------------------|----------------------------------|------------|--------------|----------|--------------|
| Size variables (in ²) | A ₃ | 2.5 | 2.61 | 2.5 | 2.7 | 2.4 | 3.8 |
| | A ₄ | 2.2 | 2.56 | 2.5 | 2.5 | 2.2 | 2 |
| | A ₅ | 0.7 | 0.69 | 0.8 | 0.7 | 1.1 | 0.4 |
| | A ₇ | 0.1 | 0.47 | 0.1 | 0.1 | 0.1 | 5 |
| | A ₈ | 1.3 | 0.8 | 0.7 | 0.9 | 1.2 | 1.5 |
| | A ₁₀ | 1.3 | 1.13 | 1.4 | 1.1 | 1.3 | 1.4 |
| | A ₁₂ | 1.8 | 1.71 | 1.7 | 1.8 | 1.7 | 2 |
| | A ₁₄ | 0.5 | 0.77 | 0.8 | 0.7 | 0.6 | 0.4 |
| | A ₁₅ | 0.8 | 1.09 | 0.9 | 0.9 | 0.8 | 0.7 |
| | A ₁₈ | 1.2 | 1.34 | 1.3 | 1.3 | 1.6 | 2 |
| | A ₂₀ | 0.4 | 0.36 | 0.3 | 0.3 | 0.3 | 1.2 |
| | A ₂₂ | 1.2 | 0.97 | 0.9 | 1.1 | 0.9 | 0.5 |
| | A ₂₄ | 0.9 | 1 | 1 | 1 | 1.2 | 1.6 |
| | A ₂₆ | 1 | 1.03 | 1.1 | 0.9 | 1 | 1.7 |
| | A ₂₇ | 3.6 | 0.88 | 5 | 0.8 | 1 | 1.1 |
| | A ₂₈ | 0.1 | 0.55 | 0.1 | 0.1 | 0.6 | 0.1 |

| | | | | | | | |
|----------------------------|------------------------|---------|--------|---------|----------|----------|----------|
| | A ₃₀ | 2.4 | 2.59 | 2.5 | 2.7 | 2.8 | 3.2 |
| | A ₃₁ | 1.1 | 0.84 | 1 | 0.8 | 0.4 | 0.4 |
| | A ₃₃ | 0.1 | 0.25 | 0.1 | 0.1 | 0.1 | 0.1 |
| | A ₃₅ | 2.7 | 2.86 | 2.8 | 3 | 2.9 | 3.1 |
| | A ₃₆ | 0.8 | 0.92 | 0.9 | 0.9 | 1.5 | 0.5 |
| | A ₃₈ | 0.1 | 0.67 | 0.1 | 0.1 | 0.6 | 0.2 |
| | A ₄₀ | 2.8 | 3.06 | 3 | 3.2 | 3.1 | 3.2 |
| | A ₄₁ | 1.3 | 1.04 | 1 | 1 | 0.9 | 0.8 |
| | A ₄₃ | 0.2 | 0.1 | 0.1 | 0.1 | 0.1 | 0.1 |
| | A ₄₅ | 3 | 3.13 | 3.2 | 3.3 | 3.3 | 3.2 |
| | A ₄₆ | 1.2 | 1.12 | 1.2 | 1.2 | 0.8 | 0.4 |
| Geometry variables (in) | x ₂ | 114 | 107.76 | 101.339 | 100.972 | 103.6063 | 120.840 |
| | x ₄ | 97 | 89.15 | 85.911 | 80.477 | 81.5008 | 88.893 |
| | y ₄ | 125 | 137.98 | 135.965 | 136.870 | 143.0525 | 160.416 |
| | x ₆ | 76 | 66.75 | 74.797 | 64.391 | 67.0169 | 58.621 |
| | y ₆ | 261 | 254.47 | 237.745 | 247.049 | 252.8466 | 289.544 |
| | x ₈ | 69 | 57.38 | 64.311 | 55.259 | 54.5203 | 37.959 |
| | y ₈ | 316 | 342.16 | 321.342 | 338.453 | 374.0126 | 397.740 |
| | x ₁₀ | 56 | 49.85 | 53.335 | 48.733 | 39.8226 | 31.208 |
| | y ₁₀ | 414 | 417.17 | 414.302 | 409.738 | 443.9461 | 444.700 |
| | x ₁₂ | 50 | 44.66 | 46.028 | 43.474 | 30.9474 | 26.371 |
| | y ₁₂ | 463 | 475.35 | 489.921 | 472.148 | 491.9941 | 473.438 |
| | x ₁₄ | 54 | 41.09 | 41.835 | 44.835 | 36.7597 | 39.436 |
| | y ₁₄ | 524 | 513.15 | 522.416 | 512.190 | 510.000 | 528.233 |
| | x ₂₀ | 1 | 17.9 | 1 | 3.842 | 17.6763 | 31.749 |
| | y ₂₀ | 587 | 597.92 | 598.391 | 591.145 | 598.8911 | 595.814 |
| | x ₂₁ | 99 | 93.54 | 97.87 | 84.504 | 77.6661 | 88.774 |
| | y ₂₁ | 631 | 623.94 | 624.055 | 630.347 | 619.89 | 603.940 |
| Results | W _{best} (Ib) | 1925.79 | 1900 | 1864.1 | 1860.161 | 1871.843 | 1852.446 |
| | Analysis | N/A | N/A | 25000 | N/A | 2850 | 6940 |

Table 12: The stress value of the 47-bar truss

| Member | Stress (Ib/in ²) | Member | Stress (Ib/in ²) | Member | Stress (Ib/in ²) |
|--------|------------------------------|--------|------------------------------|--------|------------------------------|
| 1 | 4074.45 | 17 | -14250.18 | 33 | 1664.13 |
| 2 | 5619.94 | 18 | -13485.29 | 34 | 6118.15 |
| 3 | -11577.62 | 19 | -3002.18 | 35 | -14816.69 |
| 4 | -14793.83 | 20 | -1063.73 | 36 | -2288.82 |
| 5 | 3299.14 | 21 | -8027.09 | 37 | -1767.88 |
| 6 | -2646.65 | 22 | -12405.51 | 38 | 606.69 |
| 7 | 297.15 | 23 | 12207.38 | 39 | 5414.07 |
| 8 | 4023.70 | 24 | 18865.95 | 40 | -14308.52 |
| 9 | -14601.23 | 25 | 11495.32 | 41 | -2272.12 |
| 10 | -11945.39 | 26 | 17765.49 | 42 | 1723.52 |
| 11 | -14301.81 | 27 | 18514.38 | 43 | 5887.90 |
| 12 | -14742.40 | 28 | 2459.21 | 44 | 5004.76 |
| 13 | 18872.94 | 29 | 5341.69 | 45 | -13942.00 |
| 14 | -7188.20 | 30 | -14178.08 | 46 | 348.56 |
| 15 | -6814.95 | 31 | 4676.41 | 47 | -149.44 |
| 16 | 15840.40 | 32 | -4726.63 | | |

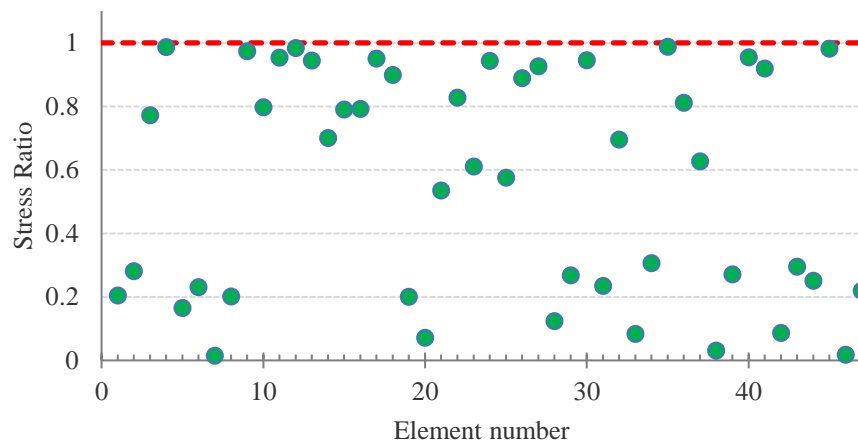


Figure 17: The stress ratio of the 47-bar truss in the optimal solution

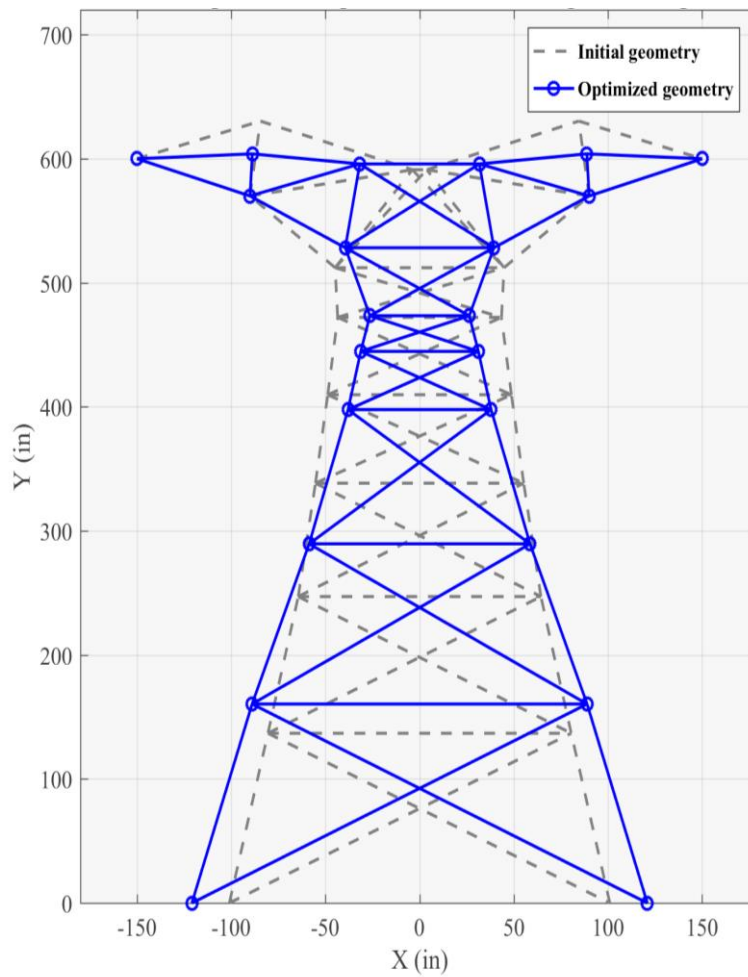


Figure 18: Initial and optimum geometry of the 47-bar truss

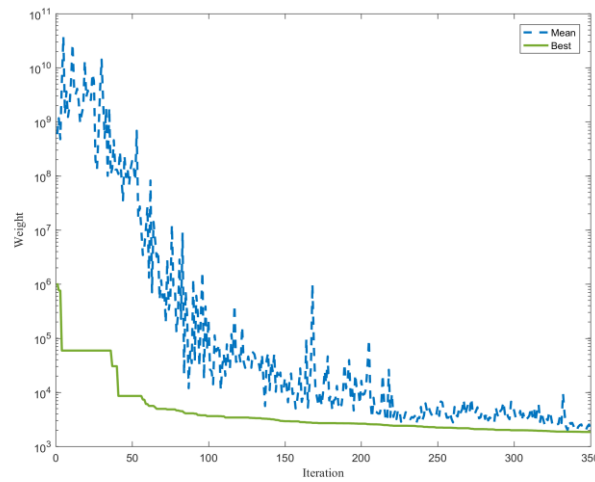


Figure 19: The convergence curve of the 47-bar truss

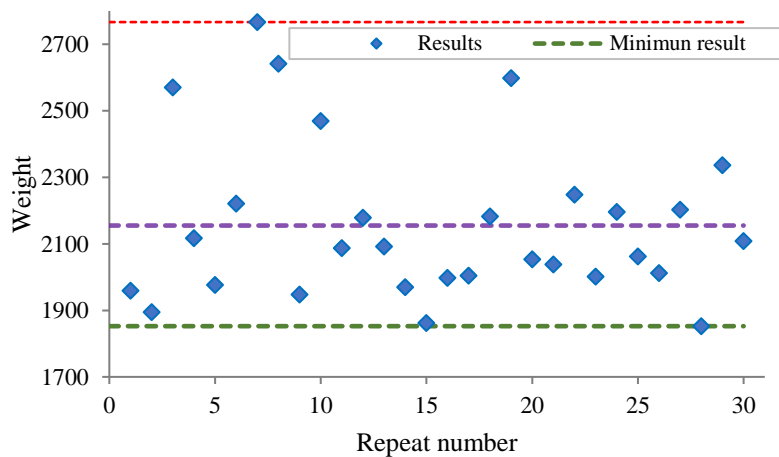


Figure 20: The optimal weight of the 47-bar truss in each independent run

5. CONCLUSIONS

In this study, the HGPG algorithm was utilized for the size and geometry optimization of truss structures. The research aimed to demonstrate the effectiveness of the HGPG algorithm in addressing combined size-geometry optimization problems. The algorithm takes into account continuous design variables for the location of joints and discrete design variables for cross-sectional areas. The main goal is to determine the optimal weight of the truss structures while satisfying local buckling, stress, and displacement constraints. The study employs a penalty function to convert a constrained problem into an unconstrained one. The HGPG was applied to four 2D and 3D benchmark examples. Comparative analysis with other optimization algorithms revealed that the HGPG is a highly effective method for such

engineering optimization problems, capable of reducing analysis costs while achieving lighter designs.

REFERENCES

1. Christensen PW, Klarbring A. An Introduction to Structural Optimization. Vol **153**. Springer Science & Business Media; 2008.
2. Kaveh A, Ilchi Ghazaan M, Bakhshpoori T. An improved ray optimization algorithm for design of truss structures. *Period Polytech Civ Eng*. 2013; **57**(2): 97-112.
3. Dehghani AA, Hamzehei-Javaran S, Shojaei S, Goodarzimehr V. Optimal analysis and design of large-scale problems using a Modified Adolescent Identity Search Algorithm. *Soft Comput*. Published online 2024.
4. Dehghani AA, Goodarzimehr V, Hamzehei-Javaran S, Shojaei S. Modified adolescent identity search algorithm for optimization of steel skeletal frame structures. *Sci Iran*. Published online 2023: 1-30.
5. SeyedOskouei SL, Sojoudizadeh R, Milanchian R, Azizian H. Shape and size optimization of truss structure by means of improved artificial rabbits optimization algorithm. *Eng Optim*. 2024; **14**(3): 355-83.
6. Dastan M, Shojaei S, Hamzehei-Javaran S, Goodarzimehr V. Hybrid teaching-learning-based optimization for solving engineering and mathematical problems. *J Brazilian Soc Mech Sci Eng*. 2022; **44**(9): 431.
7. Dastan M, Goodarzimehr V, Shojaei S, Hamzehei-Javaran S, Talatahari S. Optimal Design of Planar Steel Frames Using the Hybrid Teaching-Learning and Charged System Search Algorithm. *Iran J Sci Technol Trans Civ Eng*. Published online 2023: 1-17.
8. Biabani F, Shojaei S, Hamzehei-Javaran S. A new insight into metaheuristic optimization method using a hybrid of PSO, GSA, and GWO. In: *Structures*. Vol **44**. Elsevier; 2022: 1168-89.
9. Biabani F, Razzazi A, Shojaei S, Hamzehei-Javaran S. Design and application of a hybrid meta-heuristic optimization algorithm based on the combination of PSO, GSA, GWO and cellular automation. *Iran Univ Sci Technol*. 2022; **12**(3): 279-312.
10. Shojaei S, Arjomand M, Khatibinia M. A hybrid algorithm for sizing and layout optimization of truss structures combining discrete PSO and convex approximation. *Int J Optim Civ Eng*. 2013; **3**(1): 57-83.
11. Shahrouzi M, Taghavi AM. A modified sine-cosine algorithm with dynamic perturbation for effective optimization of engineering problems. *Int J Optim Civ Eng*. 2024; **14**(3): 385-422.
12. Darvishi P, Shojaei S. Size and geometry optimization of truss structures using the combination of DNA computing algorithm and generalized convex approximation method. *Int J Optim Civ Eng*. 2018; **8**(4): 625-56.
13. Wu SJ, Chow PT. Steady-state genetic algorithms for discrete optimization of trusses. *Comput Struct*. 1995; **56**(6): 979-91.
14. Hasańcebi O, Erbatur F. Layout optimization of trusses using improved GA methodologies. *Acta Mech*. 2001; **146**(1-2): 87-107.

15. Kaveh A, Kalatjari V. Size/geometry optimization of trusses by the force method and genetic algorithm. *ZAMM Zeitschrift für Angew Math und Mech.* 2004; **84**(5): 347-57.
16. Kaveh A, Dadras A, Montazeran AH. Chaotic enhanced colliding bodies algorithms for size optimization of truss structures. *Acta Mech.* 2018; **229**(7): 2883-907.
17. Kaveh A, Mahdavi VR. Colliding bodies optimization: a novel meta-heuristic method. *Comput Struct.* 2014; **139**: 18-27.
18. Mahdavi SH, Azimbeik K. A modified genetic algorithm strategy for optimal sensor exciter placement capable of time domain structural. *Int J Optim Civ Eng.* 2022; **12**(4): 517-43. <http://ijoe.iust.ac.ir/article-1-532-fa.pdf>
19. Mahdavi SH, Razak HA. Optimal sensor placement for time-domain identification using a wavelet-based genetic algorithm. *Smart Mater Struct.* 2016; **25**(6): 65006.
20. Yu Z, Mahdavi SH, Xu C. Time-domain spectral element method for impact identification of frame structures using enhanced GAs. *KSCE J Civ Eng.* 2019; **23**(2): 678-90.
21. Mahdavi VR, Kaveh A, Engineering G. Structural damage identification based on changes in natural frequencies using three multi-objective metaheuristic algorithms. *Int J Optim Civ Eng.* 2024; **14**(3): 337-54.
22. Vanderplaats GN. Numerical Optimization Techniques for Engineering Design: With Applications. Vol 1. McGraw-Hill New York; 1984.
23. Kennedy J, Eberhart R. Particle swarm optimization. In: Proceedings of ICNN'95-International Conference on Neural Networks. Vol 4. IEEE; 1995: 1942-8.
24. Rashedi E, Nezamabadi-Pour H, Saryazdi S. GSA: a gravitational search algorithm. *Inf Sci (Ny).* 2009; **179**(13): 2232-48.
25. Mirjalili S, Mirjalili SM, Lewis A. Grey wolf optimizer. *Adv Eng Softw.* 2014; **69**: 46-61.
26. Hwang SF, He RS. A hybrid real-parameter genetic algorithm for function optimization. *Adv Eng Informatics.* 2006; **20**(1): 7-21.
27. Tang W, Tong L, Gu Y. Improved genetic algorithm for design optimization of truss structures with sizing, shape and topology variables. *Int J Numer Methods Eng.* 2005; **62**(13): 1737-62.
28. Gholizadeh S. Layout optimization of truss structures by hybridizing cellular automata and particle swarm optimization. *Comput Struct.* 2013; **125**: 86-99.
29. Rajeev S, Krishnamoorthy CS. Genetic algorithms-based methodologies for design optimization of trusses. *J Struct Eng.* 1997; **123**(3): 350-58.
30. Yang JP. Development of genetic algorithm based approach for structural optimisation. Published online 1996.
31. Ho-Huu V, Nguyen-Thoi T, Nguyen-Thoi MH, Le-Anh L. An improved constrained differential evolution using discrete variables (D-ICDE) for layout optimization of truss structures. *Expert Syst Appl.* 2015; **42**(20): 7057-69.
32. Jawad FJK, Ozturk C, Dansheng W, Mahmood M, Al-Azzawi O, Al-Jemely A. Sizing and layout optimization of truss structures with artificial bee colony algorithm. In: *Structures*. Vol 30. Elsevier; 2021: 546-59.

33. Wu SJ, Chow PT. Integrated discrete and configuration optimization of trusses using genetic algorithms. *Comput Struct*. 1995; **55**(4): 695-702.
34. Rahami H, Kaveh A, Gholipour Y. Sizing, geometry and topology optimization of trusses via force method and genetic algorithm. *Eng Struct*. 2008; **30**(9): 2360-9.
35. Hasançebi O, Erbatur F. On efficient use of simulated annealing in complex structural optimization problems. *Acta Mech*. 2002; **157**(1-4): 27-50.
36. Salajegheh E, Vanderplaats GN. Optimum design of trusses with discrete sizing and shape variables. *Struct Optim*. 1993; **6**(2): 79-85.